Preparation of tobermorite onto flux-calcinated diatomite surface and the adsorption properties and mechanism of methylene blue

Mingyang Li[a], Zijie Ren[a,b], Huimin Gao[a,b,*], Anling Zhang[a], Zhiming Sun[c]

[a]*School of Resources and Environmental Engineering, Wuhan University of Technology, Wuhan 430070, China,*
Tel. +86-027-13971465349; email: gaohuimin1958@126.com (H. Gao), Tel. +86-0391-15716529132; email: 2330843886@qq.com (M. Li),
Tel. +86-027-15071403704; email: renzijie@whut.edu.cn (Z. Ren), Tel. +86-027-18369956020; email: zhanganling@whut.com (A. Zhang)
[b]*Hubei Key Laboratory of Mineral Resources Processing and Environment, Wuhan 430070, China*
[c]*School of Chemical and Environmental Engineering, China University of Mining and Technology, Beijing 100083, China,*
Tel. +86-010-13466774499; email: zhimingsun@cumtb.edu.cn (Z. Sun)

ABSTRACT

A diatomite-based composite adsorbent with multifunctional structures was prepared using calcinated diatomite as the raw material and CaO as the agent, where conventional hydrothermal alkaline activation was employed. The procedure resulted in a highly functionalized, porous adsorbent, whose the structure and morphology, as well as its adsorption properties on methylene blue (MB) were characterized with Fourier-transform infrared spectra, scanning electron microscope, X-ray diffraction, Brunauer–Emmett–Teller measurements. Various adsorption conditions, including adsorbent dosage, contact time, contact temperature, initial MB concentration, and pH was considered. The adsorption kinetic and thermodynamic models, and static adsorption isotherms were investigated. The tests illustrated that the highest MB absorption capacity was under higher temperature and strong alkaline conditions, which accorded with the Langmuir adsorption isotherm model and the pseudo-second-order kinetic model. The whole adsorption process was governed by physical adsorption with an endothermic spontaneous nature. The adsorption of MB molecules may be attributed to electrostatic interaction and hydrogen bonding attraction. The results indicate that the modified diatomite has great potential as an alternative low-cost material in much wider industrial application.

Keywords: Calcinated diatomite; Adsorbent; Methylene blue; Hydrothermal alkaline activation

1. Introduction

Diatomite, a natural biogenetic mineral, is mainly composed of amorphous silica and contain a few fine micropores [1], which has received attention for its unique combination of physical and chemical properties, such as high permeability, developed porous structure, large surface area, low thermal conductivity, and good thermal stability [2–5]. Although there are abundant diatomite resources in China, they typically contain many assorted impurities, which has limited the commercial application of diatomite [6,7]. Accordingly, in industrial applications, the calcination or flux calcination at high temperature is a necessary process to remove the organic matter or partly metallic oxides within and to improve the whiteness [8]. In addition, the whole structure of calcinated diatomite is effectively

* Corresponding author.

improved the permeability properties are enhanced [9]. However, after calcination (i.e., heated to a higher temperature), the porous structure of diatomite would be destroyed and the silicon group (Si–OH) on the surface of diatomite is removed, which restrained the absorption capacity of diatomite [10].

The application of diatomite as the high-grade filter aid, gas-phase adsorbent, liquid phase adsorbent, paint coating, filler, and so forth, depends heavily on its origin, so a few more efforts should be attempted to enhance its adsorption capability. There are several examples in the literature for various modifications to increase the adsorption capacities [11,12]. Zhang et al. [12] hydrothermally solidified diatomite at a low temperature and found that synthesized tobermorite had a positive effect on the porosity and strength. Tobermorite ($Ca_5Si_6O_{16}(OH)_2 \cdot 4H_2O$) is a mineral material with good ion exchange properties, which is technologically important due to its essential role in waste management [13,14]. Also, tobermorite is a new type of calcium silicate, a prominent structural feature of which is the pore canal stacked along the crystallographic axis [15], where many water and Ca^{2+} ions are contained. Zhan et al. [16] prepared a manganese-oxide-modified diatomite adsorbent by an in situ method and found that the adsorbent had perfect adsorption performance for dyes. Er [17] investigated diatomite modified by microemulsion and manganese oxide for the removal of chromium ions, and the results showed that after calcination the sorption capacities were considerably improved. To the best of our knowledge, the topic of calcinated diatomite and CaO remains nearly unexplored, and the results here indicate that tobermorite promotes perfect adsorption performance, which can expand the industrial application of calcinated diatomite.

In this work, we designed and prepared a new environmentally friendly composite absorbent based on calcinated diatomite, which has a higher removal rate and adsorption capacity compared with calcinated diatomite alone. After investigating the characteristics, the adsorption performance was studied via the adsorption isotherms and kinetics of methylene blue (MB) onto calcinated diatomite and CaO-modified calcinated diatomite (M-D). Furthermore, we proposed the probable adsorption mechanism. The objective of this study is to (i) synthesize tobermorite from calcinated diatomite by hydrothermal treatment and characterize the properties; (ii) discuss the effects of the additive mass, temperature, time, pH, and initial concentrations to obtain an optimal sample; (iii) investigate the adsorption performance of MB on hydrothermal calcinated diatomite to evaluate its potential adsorbability. MB, a cationic dye that has many applications [18], was selected as a dye adsorption model.

2. Experimental part

2.1. Material

The flux-calcinated diatomite (C-D 93.06%SiO_2, 2.2%Al_2O_3, 1.51%Fe_2O_3, and other oxides) was obtained from Linjiang, China. All aqueous solutions were prepared using deionized water and calcium oxide were purchased from Shanghai Zhenxin Reagent Co., Shanghai, China, $MB(C_{16}H_{18}ClN_3S \cdot$ 3H_2O) reagents were from Shanghai Sinopharm Chemical Reagent Co., Shanghai, China. H_2SO_4 was used as pH regulator. All reagents used were of analytical grade.

2.2. Preparation of adsorbent (M-D)

First, 8 g C-D, mixed with CaO at different concentrations (i.e., 0%–9%), was poured into a 50 mL alumina crucible. Then, distilled water was directly added to cover the powders, with a solid-liquid ratio of 1:3. Following that, all of the crucibles were put into an autoclave (Shanghai Yancheng Experimental instrument Co. Ltd., Shanghai, China), and hydrothermal reactions were carried out for 12 h at 145°C with autogenous pressure. Subsequently, the obtained samples were washed to neutral with deionized water and dried for 24 h prior to being cooled at room temperature. Finally, the samples of tobermorite onto flux-calcinated diatomite (M-D) were pulverized in a mortar and sealed for further examination.

2.3. Adsorption experiments

Batch adsorption experiments were performed, where the effects of samples mass (0.01–0.12 g), MB concentration (5–25 mg/L), and solution pH (3–11) were studied. In addition, different treatment time (0.5–60 min) for the samples in the aqueous solution of MB was also investigated to determine the adsorption kinetics of C-D and M-D. Prior to the experiments, different masses of C-D or M-D samples were added into 50 mL of MB aqueous solution. The solution pH was adjusted using 0.1 M diluted NaOH and H_2SO_4, followed by gently pouring it into a 150 mL conical flask. Thereafter, the suspension was oscillated for different minutes in a SHA-BA shaking incubator (Guohua Electric Co, Changzhou, China) at 25°C. Subsequently, the suspension was filtered and the residual MB concentration in solution was obtained at 664 nm using a V-1100D type spectrophotometer (MAPADA, Shanghai, China). The adsorption capacity and removal efficiency were obtained as follows:

$$q_e = \frac{\left[\left(C_0 - C_e \right) \times V \right]}{n} \tag{1}$$

$$\eta = \left[\frac{\left(C_0 - C_e \right)}{C_0} \right] \times 100\% \tag{2}$$

Where, q_e is the adsorption capacity at equilibrium (mg/g), C_0 refers to the initial concentration of MB (mg/L), C_e corresponds to the equilibrium concentration of MB (mg/L), V represents the volume of MB solutions and η stands for the removal efficiency at equilibrium (%).

2.4. Characterization

The phase compositions were performed using X-ray diffraction (XRD) diffractometer (Cu $K_{\alpha 1}$, AXS Co., Brook, Germany), in which the tested scanning 2q varied from 10° to 50° at 30 kV at 40 mA. Fourier-transform infrared (FT-IR) spectra were measured using a Nicolet IS-10 (Thermo Fisher Scientific Inc., Waltham, MA, USA). The morphology was

observed by scanning electron microscope (SEM, JSM-5610LV, JEOL Ltd., Japan). The Brunauer–Emmett–Teller (BET) surface area and the pore size distribution were measured from N_2 adsorption by using a Micromeritics V-Sorb 2800 surface area analyzer (Beijing, China) and a laser particle analyzer (BT-9300S, Dandong Bettersize Scientific Ltd., China), respectively. Further, the zeta potential was measured with a Nano-ZS90 analyzer (Malvern Co., Malvern, UK).

3. Results and discussion

3.1. Characterization of adsorbents

The applicability of diatomite for the MB treatment mainly depended on its porous structure. The properties of the obtained M-D were characterized by SEM, XRD, and BET measurements. Fig. 1 shows the XRD patterns of C-D and M-D powders. The XRD pattern of M-D showed several new diffraction peaks at 2θ of 7.81°, 29.06°, 29.39°, and 39.39° compared with that of C-D, which were attributed to the formation of new phase composition, calcite (JCPDS NO.39-0219) [19], and tobermorite. The SEM images of C-D and M-D are shown in Fig. 2. As can been clearly seen, after modification, more sheet-like crystals were presented and were evenly coated on the entire surface of the prepared M-D radially, which was probably due to the formation of an eddy current, and the crystal grew from the center to the periphery.

As shown in Fig. 3, the nitrogen adsorption–desorption isotherms were of type IV, which exhibited H3-type hysteresis loops [20], reflecting the existence of micropores and mesopores with narrow slit-like shapes [21]. Also, the pore size distributions consisted of smaller fine (2–10 nm) intraparticle pores and larger (10–60 nm) mesopores.

The surface properties of the adsorbent are presented in Table 1. It indicates an increase in the BET surface area and pore volume, and a decrease in the average pore size after modification. Due to the limitation of crystal growth, tobermorite was loaded on the surface of diatomite, but the pore opening formed some new micropores. There is a correlation between MB exchange capacity and the surface charge of the adsorbents. The zeta potential shows pH_{ZPC} values of C-D

were 3.1, significantly higher than that of M-D. The surface charge and its distribution are important factors, which may determine the adsorption behavior. The results of the particle size distribution are shown in Table 2. It is obvious that the M-D contains much more fine particles and the particle size D_{50} is about 30.25 μm.

3.2. Adsorption properties

In the MB adsorption process, there are various influencing factors, such as adsorbent dosage, contact time, contact temperature, initial MB concentration, and pH. We undertook the adsorption experiments under the same conditions. The adsorbent dosage is an important factor in the adsorption process. Fig. 4 shows that the MB removal rate (R%) of C-D increased slowly from 7.31% to 15.53% when the adsorbent concentration increased from 0.2 to 2.4 g/L. However, the MB removal rate of M-D increased significantly from 37.77% to 94.56%, which indicated a limited capacity for C-D to remove MB and M-D has a higher removal rate. The difference in the MB removal rate of C-D and M-D was mainly due to the tobermorite that formed on the M-D surface, which provided more effective adsorption sites, thereby resulting in the high adsorption capacity of M-D [22]. In addition, the MB removal rate of M-D increased rapidly within 0.2–0.8 g/L, above which the rate increase became noticeably slow and eventually reached a plateau.

From Fig. 5 it is clear that the MB removal rate of both C-D and M-D significantly decreased with the increased initial MB concentration, which was mainly caused by the higher initial MB concentration, meaning that there were more MB molecules in solution, and correspondingly, the removal rate was decreased when the sample amount of remained unchanged [23]. Especially, the removal rate of M-D was always higher than that of C-D at the corresponding initial concentration of MB. Furthermore, the adsorption capacity of C-D increased from 1.30 to 1.67 mg/g while the M-D increased from 4.82 to 12.55 mg/g, which also demonstrated the higher adsorption capacity of M-D than C-D.

The dependency of the MB adsorption on pH is shown in Fig. 6. It is obvious that the MB removal of C-D and M-D
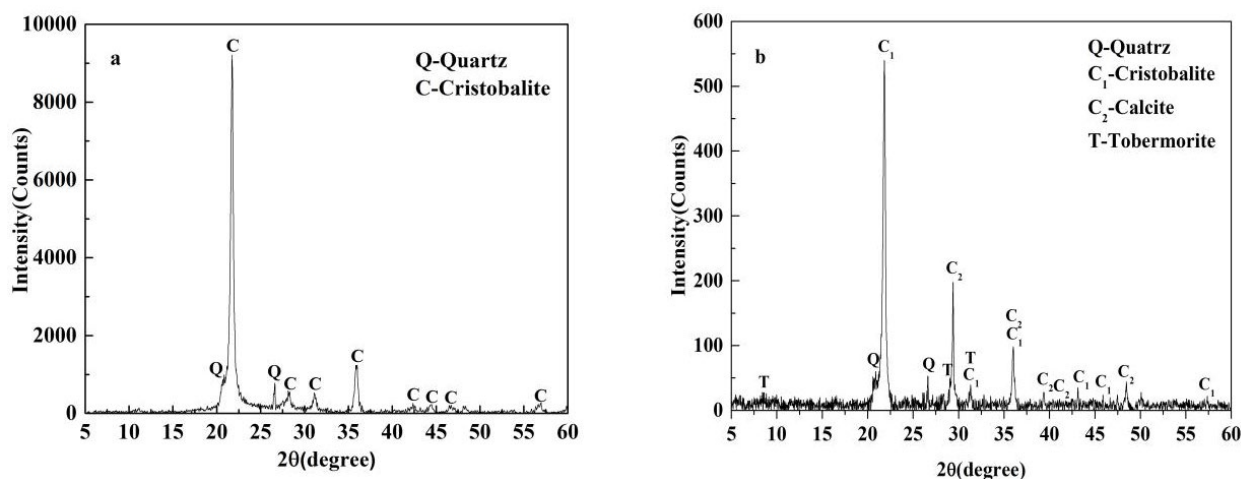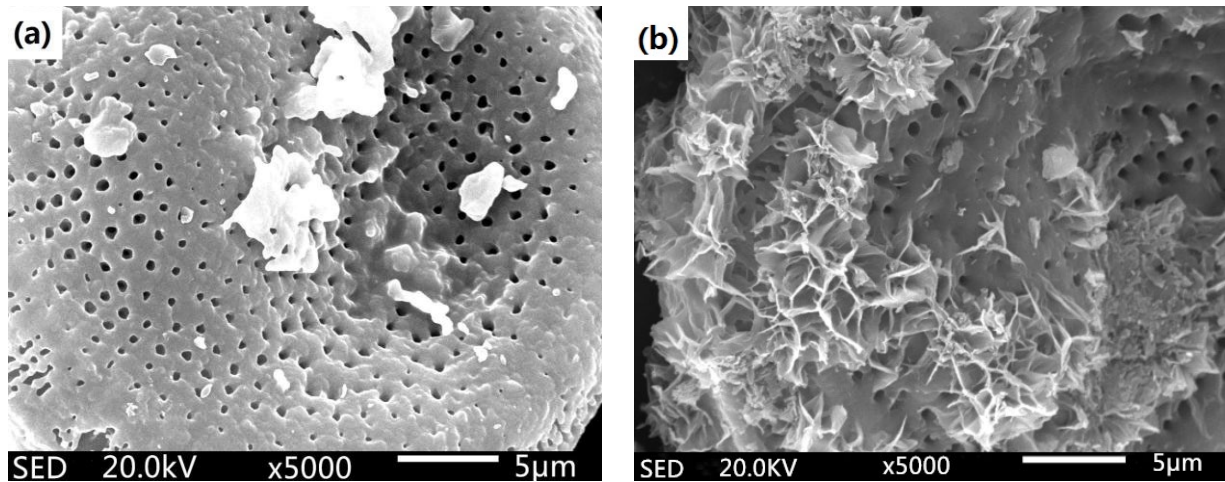

Fig. 1. XRD patterns of (a) C-D and (b) M-D.

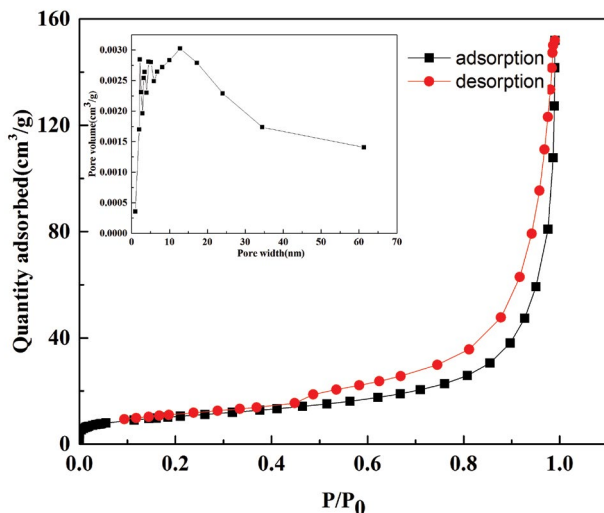Fig. 2. SEM image of (a) C-D and (b) M-D.

Fig. 3. N$_2$ adsorption–desorption isotherms and micropore size distribution of M-D.

Table 1
Surface properties of C-D and M-D

Samples	C-D	M-D
Pore volume(mm^3 g^{-1})	3.50	236.28
Average pore radius (nm)	2.53	2.05
Surface area (m^2 g^{-1})	0.87	37.28
PH$_{ZPC}$	3.1	<3

Table 2
Particle size distribution of C-D and M-D

Samples	C-D	M-D
D$_{10}$/μm	13.45	13.40
D$_{25}$/μm	24.68	20.71
D$_{50}$/μm	42.27	30.25
D$_{75}$/μm	71.72	39.83
D$_{97}$/μm	183.1	58.47

pH may be explained by the competition between the H$^+$ and MB molecules [24]. Moreover, when the pH was 9, the MB removal efficiency of C-D was 29.29%, whereas the M-D can reach 68%.

It can be observed in Fig. 7 that the increased temperature resulted in a higher MB removal rate for M-D. Moreover, the MB removal rate increased rapidly within 15 min, but after further increasing the contact time, the adsorption rate slowed down. The occurrence of such a high removal rate within a short span of time was likely due to the presence of a large number of adsorption sites on the uncovered M-D surface, which provided a stronger driving force along with the more adsorbable areas. Eventually, removal rates of 56.2%, 58.24%, 59.7%, and 61.92% were observed when the temperature increased from 20°C to 40°C over the course of 60 min, respectively. Similarly, the equilibrium adsorption capacity of M-D was also enhanced with the increased temperature, indicating that MB adsorption on M-D was an endothermic process. Especially, the adsorption capacity gradually slowed down and was close to equilibrium at 15 min, which could be attributed to the reduction of adsorption sites on the M-D prolonging the adsorption time [25].

3.3. Kinetic model analysis

In this study, two well-known kinetic models, the pseudo-first-order and pseudo-second-order models were used to investigate the adsorption dynamics on M-D and C-D [26,27] based on the experimental data.
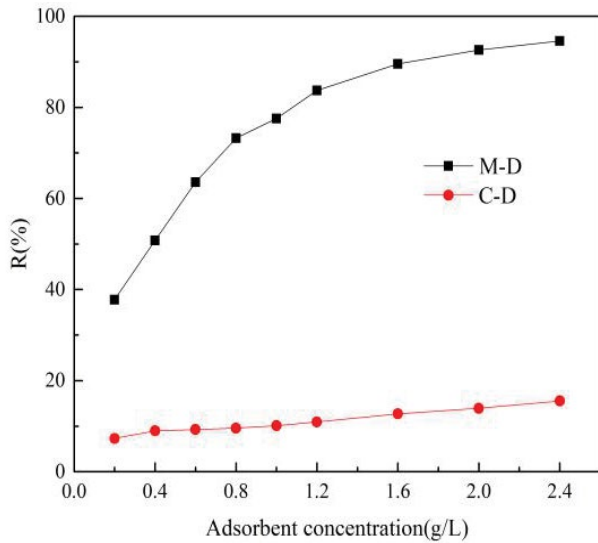
presented the same behavior, in which the removal ability gradually increased in the pH range of 3.0–9.0, above which the MB removal ability of M-D achieved a plateau yet the C-D declined. The reason for this was that above the pH$_{zpc}$ of the adsorbent, the negative charge on its surface increased, which favored the electrostatic attraction between the positively charged dye (MB$^+$) and the negatively charged. Further, the low removal of MB at a lower

Fig. 4. Effect of different dosages on the MB removal of C-D and M-D (Experimental conditions: initial MB concentration = 10 mg/L; V_{total} = 0.05 L; T = 25°C; agitation speed = 150 rpm; adsorption time = 30 min).
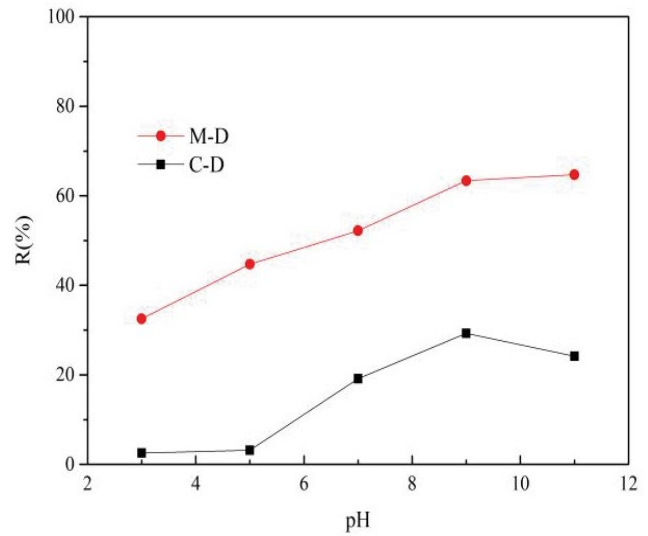

Fig. 6. Effect of pH on the MB removal of C-D and M-D (Experimental conditions: initial concentration = 10 mg/L; adsorbent dosage = 0.8 g/L; V_{total} = 0.05 L; T = 25°C; agitation speed = 150 rpm; adsorption time = 30 min).

where K_2 (g mg^{-1} min^{-1}) is the rate constant of the pseudo-second-order model.

The fitting linear plots of the first- and second-order kinetic models are shown in Fig. 8. It can be seen that the pseudo-second-order kinetic curve in Fig. 8b is a straight line, indicating the adsorption agreed with the pseudo-second-order kinetic model.

The kinetics adsorption results are shown in Table 3. For M-D, the correlation coefficient (R^2 = 0.9998) of the pseudo-second-order adsorption model was higher than that of the pseudo-first-order adsorption model, and the adsorption capacity was calculated to be 10.31 mg/g through the pseudo-do-second-order adsorption model, which was close to that determined by experimental data (10.36 mg/g). Therefore, the pseudo-second-order adsorption model should be used to describe the MB removal ability on M-D. Similarly, the pseudo-second-order adsorption model was suited for the adsorption process of MB, which corresponded with Yan's study [28].
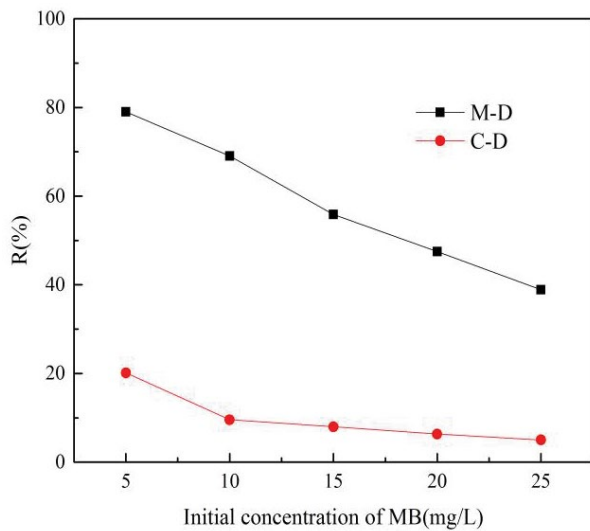

Fig. 5. Effect of the initial concentrations on the MB removal of C-D and M-D (Experimental conditions: adsorbent dosage = 0.8 g/L; V_{total} = 0.05 L; T = 25°C; agitation speed = 150 rpm; adsorption time = 30 min).

The linear form of the pseudo-first-order model was as follows:

$$\ln\left(q_e - q_t\right) = \ln q_e - K_1 t \tag{3}$$

where K_1 (min^{-1}) is the reaction rate constant.

The Eq. (4) of the pseudo-second-order kinetic model was as follows:

$$\frac{t}{q_t} = \frac{1}{K_2 q_e^2} + \frac{1}{q_e} t \tag{4}$$

3.4. Adsorption isotherms

Adsorption isotherms indicate the distribution of adsorbate molecules between the liquid and solid phases when adsorption reaches an equilibrium state. The analysis of the isotherm data by fitting them to different isotherm models is an important step in finding a suitable model. Three isotherm equilibrium models—Langmuir [29], Freundlich [30], and Temkin [31] were used to analyze the equilibrium data for M-D and C-D at 25°C. Fig. 9 shows the linear plots obtained by the three models. It can clearly be seen from Table 4 that the fitting degrees (R^2) of the Langmuir isotherms for M-D and C-D were 0.9993 and 0.9917, respectively, which were higher than those of the other two isotherm models, revealing that the MB adsorption processes on M-D and C-D were consistent with the Langmuir isotherm equilibrium model.
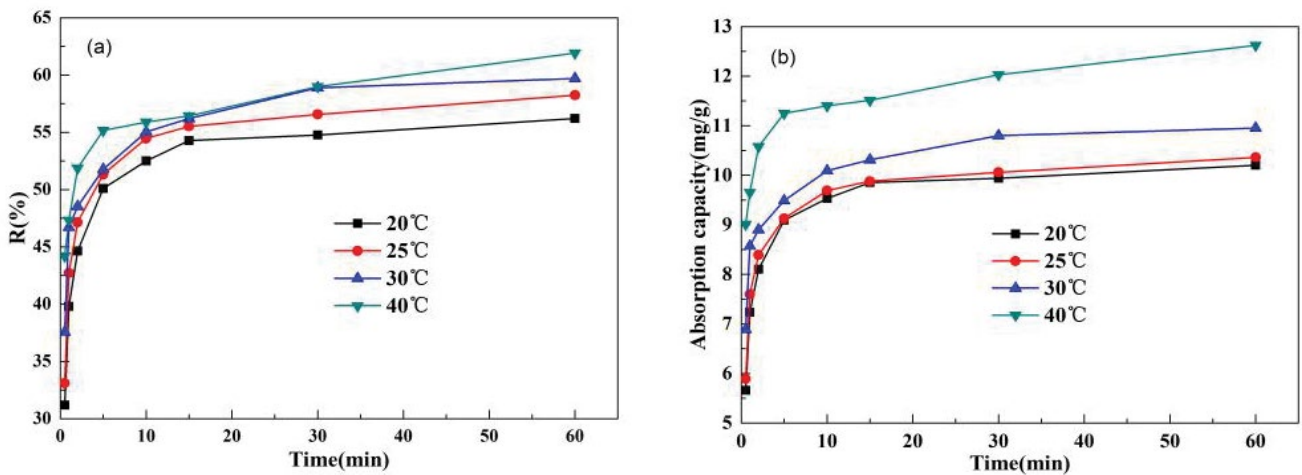
Fig. 7. Effect of time and temperature on (a) removal rate and (b) capacity of MB by M-D (Experimental conditions: adsorbent dosage = 0.8 g/L; V_{total} = 0.05 L; agitation speed = 150 rpm).
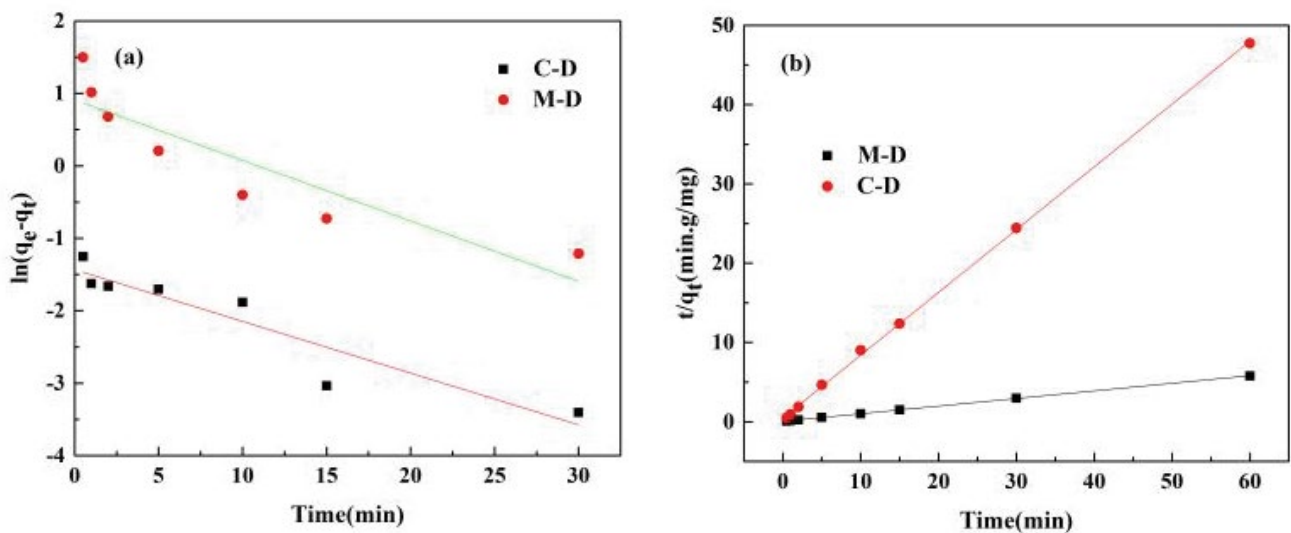

Fig. 8. Kinetic model for the adsorption of MB: (a) first-order kinetic model and (b) second-order kinetic model.

According to the adsorption characteristics of the Langmuir isotherm model [12], the MB adsorption processes on C-D and M-D were mainly homogeneous mono-molecular-layer adsorption, and the adsorbed MB molecules were not influenced by each other.

3.5. Thermodynamic studies

The thermodynamic parameters provide in-depth information about the energetic changes associated with the adsorption process. Thermodynamic data, namely enthalpy (ΔH) and entropy (ΔS) can be obtained from the slope and intercept from Fig. 10, respectively.

shows the thermodynamic properties of MB adsorption on M-D based on the van't Hoff equation. All of the Gibbs' free energy (ΔG) values at different temperatures were negative, indicating that the adsorption of MB onto M-D was a spontaneous process. Moreover, the values of ΔH were

always positive, suggesting an endothermic nature for the adsorption of MB onto M-D, which was previously confirmed by the above-discussed temperature experiment results (shown in Fig. 7). Specifically, Table 5 shows the values of all ΔH were lower than 40 kJ/mol, which confirms physical adsorption played an important role in MB absorption on M-D. Finally, from the positive value of ΔS, it could be inferred that the affinity of the M-D adsorbent to MB was a result of the increasing randomness at the interface between solid and liquid phases during adsorption.

3.6. Mechanism of adsorption

Tobermorite, a naturally existing hydrous calcium silica in calc-silicate rocks, contains silanol groups that spread over the matrix of silica. Some hydrogens are attached to oxygens, taking part in the Si–O chains [32]. The silanol group is an active one that tends to react with many polar

Table 3
Kinetic parameters for MB by M-D and C-D

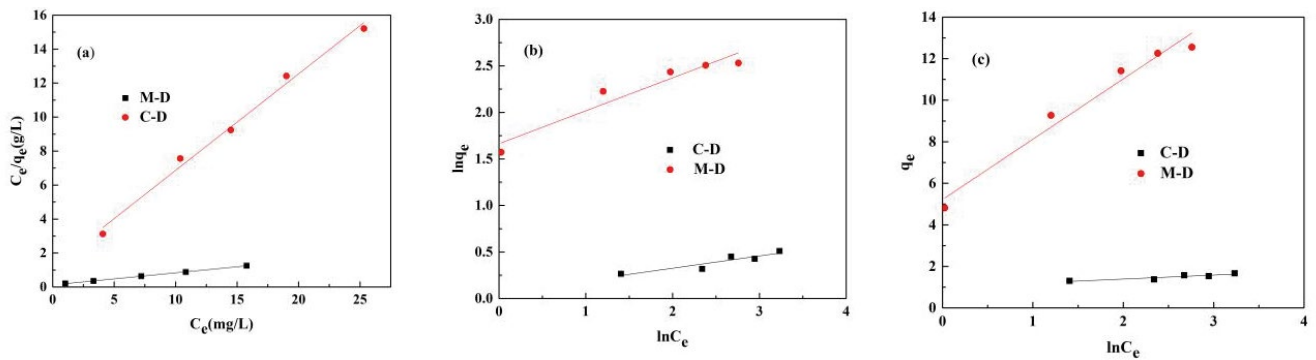| Model	Equation	Sample	Parameters		
			K_1	q_e	R^2
Pseudo-first-order	$\ln(q_e - q_t) = \ln q_e - K_1 t$	M-D	−0.0835	10.36	0.8201
		C-D	0.0355	1.35	0.8472
			K_2	q_e	R^2
Pseudo-second-order	$t/q_t = 1/K_2 q_e^2 + 1/q_e \cdot t$	M-D	0.0960	10.36	0.9998
		C-D	0.7401	1.35	0.9971

Fig. 9. Analog results for the MB adsorption on M-D and C-D based on different models: (a) Langmuir, (b) Freundlich, and (c) Temkin.

Table 4
Parameter calculation results of the three isotherm equilibrium models

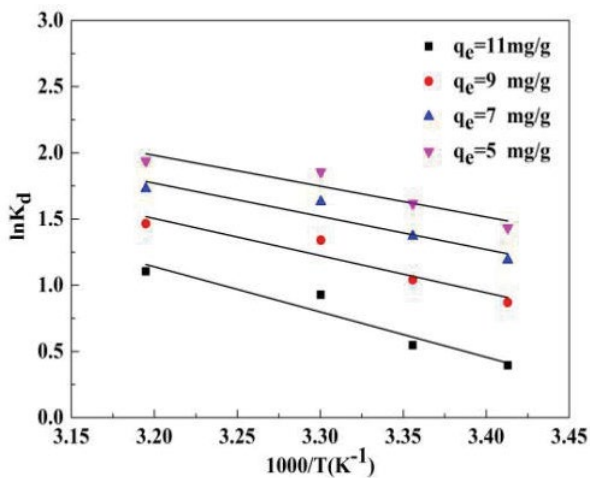| Equation	Langmuir			Freundlich			Temkin		
	$C_e/q_e = 1/K_L q_{max} + C_e/q_{max}$			$\ln q_e = \ln C_e/n + \ln K_F$			$q_e = B_1 \ln K_t + B_1 \ln C_e$		
	q_e	K_L	R^2	K_F	$1/n$	R^2	B_1	K_t	R^2
M-D	12.55	0.457	0.9993	5.276	0.354	0.9276	2.90	6.043	0.9703
C-D	1.76	0.4802	0.9917	1.0640	0.1318	0.8626	0.1926	183.3356	0.8498

Fig. 10. Fitted changed to curves of standard enthalpy and standard entropy for MB adsorption on M-D.

organic compounds and various functional groups [33]. The FT-IR spectra (Fig. 11) were recorded to investigate the possible interactions between the MB and the active groups in the adsorbent surface. A broad peak between 3,200 and 3,700 cm⁻¹ was attributed to O–H stretching, and the band at around 1,634 cm⁻¹ corresponded to the H–O–H bending vibration of water, which was caused by the presence of physically adsorbed water molecules retained in the samples [34,35]. The distinct peaks at 2,700–3,000 cm⁻¹ can be attributed to the groups of MB, such as –CH₃ and–CH₂–. The bands at 1,000–1,200 cm⁻¹ were due to the siloxane (–Si–O–Si–) group, and after the adsorption of MB, the peaks also slightly shifted, which reflects the interactions with the MB molecules. In addition, it is clear, the intensity of the 3,434 cm⁻¹ peak increased from MB adsorption, which represents the hydroxyl group absorption [36]. After adsorbing MB, there were no new absorption peaks, and a red shift occurred at around 1,634 and 1,618 cm⁻¹. This suggests interactions between the MB molecules and the silanol groups and can be interpreted as physical adsorption by hydrogen

Table 5
Thermodynamic parameters for MB absorption on M-D

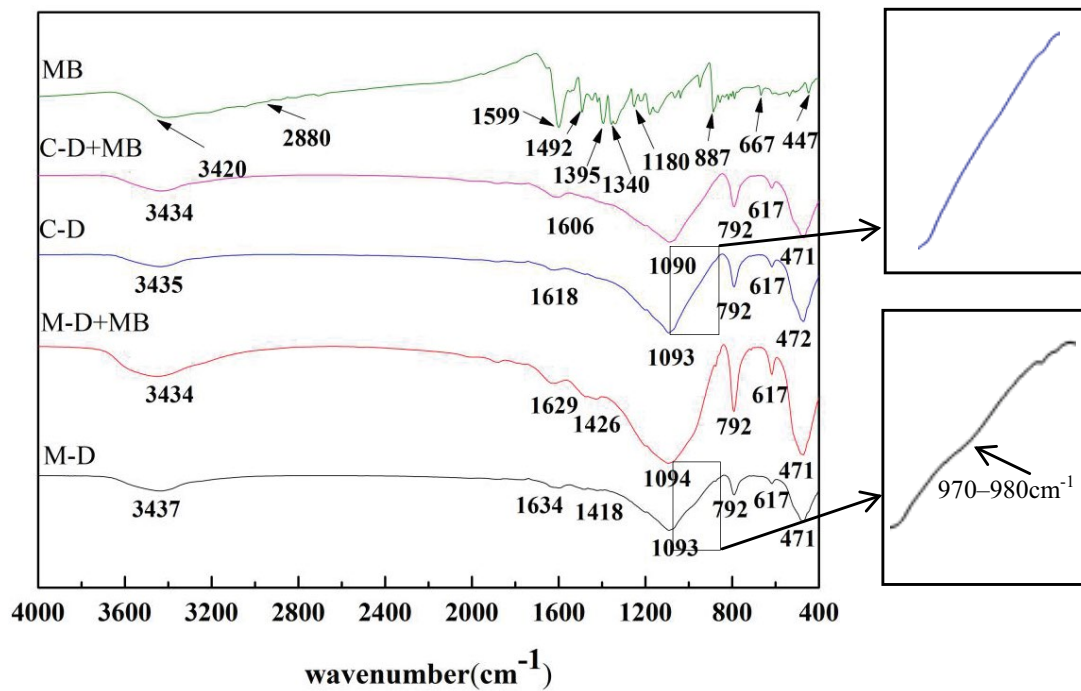| q_e (mg/g)	ΔH (kJ/mol)	ΔS (J/mol K)	ΔG (kJ/mol)			
			293 K	298 K	303 K	313 K
11	28.38	100.27	−1.00	−1.02	−1.04	−1.07
9	23.30	87.05	−2.21	−2.25	−2.28	−2.36
7	20.81	81.33	−3.02	−3.07	−3.12	−3.23
5	19.34	78.37	−3.62	−3.69	−3.75	−3.87

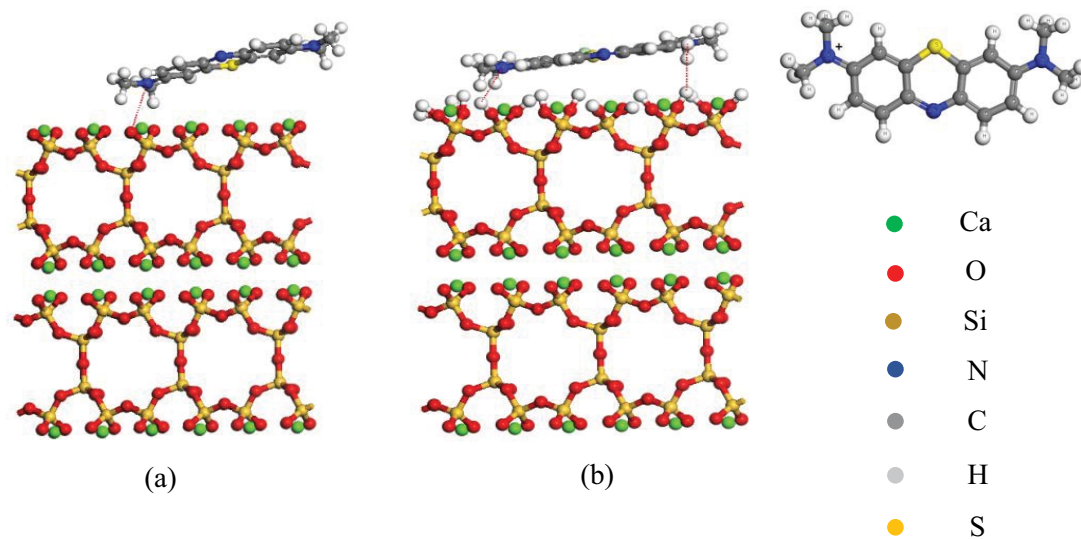Fig. 11. Infrared spectra of C-D and M-D before and after adsorbed MB.

Fig. 12. Proposed mechanism for adsorption of methylene blue onto surface groups of tobermorite and their interactions with MB molecules:(a) electrostatic interaction and (b) hydrogen bond.

bonds [37,38]. There was a weak broad-band at 970–980 cm⁻¹ assigned to the characteristic peak of tobermorite [39]. It is worth mentioning that, probably due to the larger peak at 1,093 cm⁻¹, its intensity was hindered. Further, after modification with CaO, a new peak appeared at 1,418 cm⁻¹, which corresponded to the characteristic adsorption peak of calcium carbonate [40,41], indicating the formation of calcite, which is consistent with the results of XRD.

Two mechanisms of MB adsorption onto M-D are possible: (i) adsorption by an electrostatic force of the anionic groups of rich sites on the adsorbent surface and the positive charge of the dye (MB⁺), and (ii) the hydrogen bonding interaction between the nitrogen atoms in the MB molecules and the hydroxy groups on the adsorbent surface. It is speculated that the synthesized tobermorite contributed to the adsorption of MB. More particularly, the cationic species of MB could react with Si–OH species on the surface of tobermorite in the above mentioned two ways. MB is a basic dye and, therefore is expected to interact strongly with the anionic head groups. Tobermorite, the structure is built up of complex layers, flanked on both sides by wollastonite-like chains. The calcium octahedra share oxygens with the silicate tetrahedra as a three-silicate tetrahedra repeat unit. The composite layers are bound together by an interlayer containing calcium ions and water molecules. The schematic representation of MB adsorption onto the adsorbent surface is presented in Fig. 12. The OH• groups can be divided into isolated free silanol (–Si–OH) and geminal free silanol (HO–Si–OH), which can act as centers for adsorption by forming hydrogen bonds with the nitrogen atoms in MB molecules.

4. Conclusion

In this study, a diatomite-based adsorbent (M-D) with excellent adsorption capacity was successfully prepared, and newly formed tobermorite was synthesized onto the M-D surface. The synthesized M-D showed a relatively higher BET value and a bigger pore volume compared with that of C-D. In addition, the MB adsorption behavior on C-D and M-D was investigated in this study. Various measurements indicate that the MB absorption capacity of M-D was significantly higher than that of C-D, most likely due to the increase of the electrostatic attraction between positively charged MB and the more negative M-D particles when tobermorite was formed on the C-D surface. Further adsorption equations indicated that the adsorption processes obeyed the pseudo-second-order model, with a spontaneous endothermic process under all conditions. Moreover, the MB adsorption on M-D was also well-fitted by the Langmuir adsorption process, with a maximum monolayer adsorption capacity of 10.36 mg/g at 15°C.

The mechanism possibly involves electrostatic interaction and hydrogen bonding interaction. The hydrothermal synthesis of tobermorite exerts a positive effect on porosity and favors the removal of MB with good mechanical properties during the adsorption process. Therefore, in light of the findings of this study, M-D can be suggested as an excellent semifinished material alternative to C-D for industrial productions or applications, like high-grade filter aid, gas-phase adsorbent, liquid phase adsorbent, paint coating, filler, etc.

References

[1] M.S. Wang, L.Z. Fan, M. Huang, J. Li, X. Qu, Conversion of diatomite to porous Si/C composites as promising anode materials for lithium-ion batteries, J. Power Sources, 219 (2012) 29–35.

[2] E. Erdem, G. Çölgeçen, R. Donat, The removal of textile dyes by diatomite earth, J. Colloid Interface Sci., 282 (2005) 314–319.

[3] S. Guodong, H. Jun, W. Xiangke, Sorption properties of Th(IV) on the raw diatomite--effects of contact time, pH, ionic strength and temperature, Appl. Radiat. Isot., 66 (2008) 1313–1320.

[4] A.F.D.D. Namor, A.E. Gamouz, S. Frangie, V. Martinez, L. Valiente, O.A. Webb, Turning the volume down on heavy metals using tuned diatomite. A review of diatomite and modified diatomite for the extraction of heavy metals from water, J. Hazard. Mater., 241–242 (2012) 14–31.

[5] B. Yılmaz, N. Ediz, The use of raw and calcined diatomite in cement production, Cem. Concr. Compos., 30 (2008) 202–211.

[6] L. Xiao, B. Pang, Experimental Study on Purification of Low Grade Diatomite, IOP Conference Series: Earth and Environmental Science, Volume 61, 3rd International Conference on Energy Materials and Environmental Engineering, Bangkok, Thailand, 2017.

[7] Z. Sun, X. Yang, G. Zhang, S. Zheng, R.L. Frost, A novel method for purification of low grade diatomite powders in centrifugal fields, Int. J. Miner. Process., 125 (2013) 18–26.

[8] Z. Ren, H. Gao, H. Zhang, L. Xi, Effects of fluxes on the structure and filtration properties of diatomite filter aids, Int. J. Miner. Process., 130 (2014) 28–33.

[9] N. Ediz, İ. Bentli, İ. Tatar, Improvement in filtration characteristics of diatomite by calcination, Int. J. Miner. Process., 94 (2010) 129–134.

[10] Y. Sabriye, G. Erenturk, A. Sule, Adsorptive removal of thorium (IV) using calcined and flux calcined diatomite from Turkey: evaluation of equilibrium, kinetic and thermodynamic data, Appl. Clay Sci., 67–68 (2012) 106–116.

[11] J.H. Li, Z.Q. Chi, H.F. Chen, Synthesis of NaY zeolite molecular sieves from calcined diatomite, Adv. Mater. Res., 236–238 (2011) 362–368.

[12] Y. Zhang, Z. Jing, Y. Li, J. Fan, W. Kan, Hydrothermal synthesis of tobermorite from diatomite and its adsorption performance for methylene blue, Mater. Res. Innov., 19 (2015) S2–S63.

[13] H. Qi, D. Hai, S.P. Liang, C. Yin, Study on Adsorption of Pb²⁺ by Synthetic Tobermorite, International Conference on Mechanic Automation and Control Engineering, Wuhan, China, 2010.

[14] M. Monasterio, J.J. Gaitero, H. Manzano, J.S. Dolado, S. Cerveny, Effect of chemical environment on the dynamics of water confined in calcium silicate minerals: natural and synthetic tobermorite, Langmuir ACS J. Surf. Colloids, 31 (2015) 4964–4972.

[15] S. Shaw, S.M. Clark, C.M.B. Henderson, Hydrothermal formation of the calcium silicate hydrates, tobermorite (Ca₅Si₆O₁₆(OH)₂·4H₂O) and xonotlite (Ca₆Si₆O₁₇(OH)₂): an in situ synchrotron study, Chem. Geol., 167 (2000) 129–140.

[16] S. Zhan, J. Lin, M. Fang, X. Qian, Preparation of manganese oxides-modified diatomite and its adsorption performance for dyes, Rare Metal Mater. Eng., 39 (2010) 397–400.

[17] L.I. Er, X. Zeng, Y. Fan, Removal of chromium ion (III) from aqueous solution by manganese oxide and microemulsion modified diatomite, Desalination, 238 (2009) 158–165.

[18] J. Zhang, Q. Ping, M. Niu, H. Shi, L.I. Na, Kinetics and equilibrium studies from the methylene blue adsorption on diatomite treated with sodium hydroxide, Appl. Clay Sci., 84 (2013) 12–16.

[19] A. Samanta, D.K. Chanda, P.S. Das, J. Ghosh, A. Dey, S. Das, A.K. Mukhopadhyay, Synthesis of mixed calcite calcium oxide nanojasmine flowers, Ceram. Int., 42 (2016) 2339–2348.

[20] X.M. Liu, M.G.Q. Lu, Z.F. Yan, A novel method to prepare mesoporous nano-zirconia, Stud. Surf. Sci. Catal., 146 (2003) 239–242.

[21] J. Kim, K.C. Song, S. Foncillas, S.E. Pratsinis, Dopants for synthesis of stable bimodally porous titania, J. Eur. Ceram. Soc., 21 (2001) 2863–2872.

[22] L. Jiang, L. Liu, S. Xiao, J. Chen, Preparation of a novel manganese oxide-modified diatomite and its aniline removal mechanism from solution, Chem. Eng. J., 284 (2016) 609–619.

[23] R. Zheng, H. Gao, J. Guan, Z. Ren, J. Tian, Characteristics of cationic Red X-GRL adsorption by diatomite tailings, J. Wuhan Univ. Technol.-Mater. Sci. Ed., 32 (2017) 1038–1047.

[24] M.A.M. Khraisheh, M.A. Al-Ghouti, S.J. Allen, M.N. Ahmad, Effect of OH and silanol groups in the removal of dyes from aqueous solution using diatomite, Water Res., 39 (2005) 922–932.

[25] R.K. Sheshdeh, S. Abbasizadeh, M.R.K. Nikou, K. Badii, M.S. Sharafi, Liquid Phase adsorption kinetics and equilibrium of toluene by novel modified-diatomite, J. Environ. Health Sci. Eng., 12 (2014) 148.

[26] Y.S. Ho, J.C.Y. Ng, G. Mckay, Kinetics of pollutant sorption by biosorbents: review, Sep. Purif. Methods, 29 (2000) 189–232.

[27] M. Özacar, Equilibrium and kinetic modelling of adsorption of phosphorus on calcined alunite, Adsorption, 9 (2003) 125–132.

[28] Y. Shu, W. Huo, J. Yang, X. Zhang, Q. Wang, W. Lu, Y. Pan, H. Yong, Green synthesis and influence of calcined temperature on the formation of novel porous diatomite microspheres for efficient adsorption of dyes, Powder Technol., 329 (2018) S806459080.

[29] L. Dong, Y. Peng, T. Daoyong, L. Hongmei, F. Mingde, Y. Aihua, Z. Jianxi, H. Hongping, Effects of inherent/enhanced solid acidity and morphology of diatomite templates on the synthesis and porosity of hierarchically porous carbon, Langmuir ACS J. Surf. Colloids, 26 (2010) 18624–18627.

[30] Z.W. Luo, Z. Chen, S.H. Liu, A study on adsorption ammonia nitrogen of diatomite modified by microwave, Adv. Mater. Res., 602–604 (2013) 1211–1214.

[31] B.K.S.R. Srikrishnaperumal, Biosorption of crystal violet onto *Cyperus rotundus* in batch system: kinetic and equilibrium modeling, Desal. Water Treat., 52 (2014) 3535–3546.

[32] H.D. Megaw, C.H. Kelsey, Crystal structure of tobermorite, Nature, 177 (1956) 390–391.

[33] J.X. Lin, L. Wang, Adsorption of dyes using magnesium hydroxide-modified diatomite, Desal. Water Treat., 8 (2009) 263–271.

[34] S. Yusan, K. Korzhynbayeva, S. Aytas, S. Tazhibayeva, K. Musa-bekov, Preparation and investigation of structural properties of magnetic diatomite nanocomposites formed with different iron content, J. Alloys Compd., 608 (2014) 8–13.

[35] D.L. Zhao, S.J. Feng, C.L. Chen, S.H. Chen, D. Xu, X.K. Wang, Adsorption of thorium(IV) on MX-80 bentonite: effect of pH, ionic strength and temperature, Appl. Clay Sci., 41 (2008) 23.

[36] M.A.M. Khraisheh, M.S. Alg-Houti, Enhanced dye adsorption by microemulsion-modified calcined diatomite (µE-CD), Adsorption, 11 (2005) 547–559.

[37] Y. Wang, M. Muhler, W.L. Ch, Spectroscopic evidence for the partial dissociation of H_2O on ZnO(1010), Phys. Chem. Chem. Phys., 8 (2006) 1521–1524.

[38] C.H. Fan, Y.C. Zhang, Study on the co-adsorption mechanism of Pb (II) and chlorpyrifos on arid loess in northwestern China, Spectrosc. Spectral Anal., 33 (2013) 2137–2142.

[39] P. Long, J. Chen, J. Li, L. Tongjian, Structure and characterization of novel tobermorite, Eng. Plast. Appl., (2016).

[40] L. Qiang, L. Guo, Y. Zhou, Y. Dai, L. Feng, J. Zhou, J. Zhao, J. Liu, G. Qian, Phosphate adsorption on biogenetic calcium carbonate minerals: effect of a crystalline phase, Desal. Water Treat., 47 (2012) 78–85.

[41] S. Gunasekaran, G. Anbalagan, Spectroscopic characterization of natural calcite minerals, Spectrochim. Acta, Part A, 68 (2007) 656–664.